Geophysical Journal International

Geophys. J. Int. (2014) **196,** 1351–1364
Advance Access publication 2013 December 17

doi: 10.1093/gji/ggt470

The inability of magnetotelluric off-diagonal impedance tensor elements to sense oblique conductors in three-dimensional inversion

Duygu Kiyan,[1,2] Alan G. Jones[1] and Jan Vozar[1]

[1]*Geophysics Section, School of Cosmic Physics, Dublin Institute for Advanced Studies, Dublin 2, Ireland. E-mail: duygu@cp.dias.ie*
[2]*Department of Earth and Ocean Sciences, National University of Ireland, Galway, Ireland*

Accepted 2013 November 19. Received 2013 October 10; in original form 2013 July 4

SUMMARY

In this paper, we use synthetic data sets from a profile to demonstrate the importance of aligning the 3-D mesh and data coordinate system with the dominant geo-electrical strike direction in 3-D inverse modelling. The resistivity model investigated consists of a regional, elongated 2-D conductive structure at 45° to the profile. We compare the results of full impedance tensor inversion with the results from inversion of only off-diagonal components of the magnetotelluric impedance tensor. The 3-D inversion result obtained with the complete tensor elements yields the subsurface model closest to the original model, whereas the result of inverting only off-diagonal components is the poor imaging of the continuity of the conductive 2-D body. However, the conductor can be correctly recovered using only the off-diagonal components if the model mesh and the data are aligned with quasi-2-D geo-electrical strike.

Key words: Numerical solutions; Inverse theory; Magnetotellurics.

1 INTRODUCTION

In recent years, with the availability of 3-D inversion codes (e.g. Farquharson *et al.* 2002; Siripunvaraporn *et al.* 2005a; Egbert & Kelbert 2012), routine applications of 3-D inverse modelling of magnetotelluric (MT) data have become common in the EM community. However, logistics, acquisition costs and instrumentation availability still require MT field specialists to acquire data predominantly along 2-D profiles across geological terranes. One of the motivations for applying 3-D inversion instead of 2-D inversion is that no assumption about geo-electric strike direction or coordinate system has to be made. In some cases, it is difficult to determine a common geo-electric strike angle for whole period range and for all sites along the 2-D profile (e.g. Marquis *et al.* 1995; Kiyan *et al.* 2010; Miensopust *et al.* 2011). Siripunvaraporn *et al.* (2005b) demonstrated the advantages of interpretation of 2-D MT profile data using 3-D inversion (Siripunvaraporn *et al.* 2005a) for a synthetic data set. Siripunvaraporn *et al.* (2005b) conclude that 3-D inversion of single profile data can provide a more meaningful picture of the subsurface geometry beneath the profile, particularly when using the full complete impedance tensor. Xiao *et al.* (2010), Patro & Egbert (2011), Bertrand *et al.* (2012), and Khoza *et al.* (2013) present their 3-D models from MT profile field data set. Among these, Patro & Egbert (2011) present inversion results with data and a 3-D model grid aligned with the predominant geological strike direction of the study area, in order to force structures to have longer length scales along the strike direction. In addition, they compare full impedance tensor inversion results with results from only off-diagonal components, and they concluded that the main structural features inferred from 2-D and 3-D modelling are in good agreement, although there are differences regarding the positions and amplitudes of the main conductive features in the resulting models, particularly in the use of higher smoothing scale along geo-electric strike direction. Most recently, Tietze & Ritter (2013) investigated the influence of the orientation of the inversion coordinate system, data error bounds and model regularization parameters, including using different components of the impedance tensor in the context of inverting a large, real 2-D array and complementary synthetic data sets via 3-D inversion. Our paper results from an examination of the differences found when applying 3-D compared to 2-D inversion.

In this paper, we present the limitations of 3-D interpretation of single MT profile data in the presence of a regional 2-D structure with a strongly oblique strike direction (45°) to the adopted 3-D grid. Our aims are (1) to demonstrate the importance of including the diagonal terms of the impedance tensor ($\mathbf{Z}_{xx}$, $\mathbf{Z}_{xy}$, $\mathbf{Z}_{yx}$, $\mathbf{Z}_{yy}$), and (2) to consider using a strike-aligned coordinate system when using off-diagonal impedance tensor elements ($\mathbf{Z}_{x'y'}$, $\mathbf{Z}_{y'x'}$) to map the right geometry and shape of the conductive structures, as most 3-D structures will have a dominant length direction with quasi

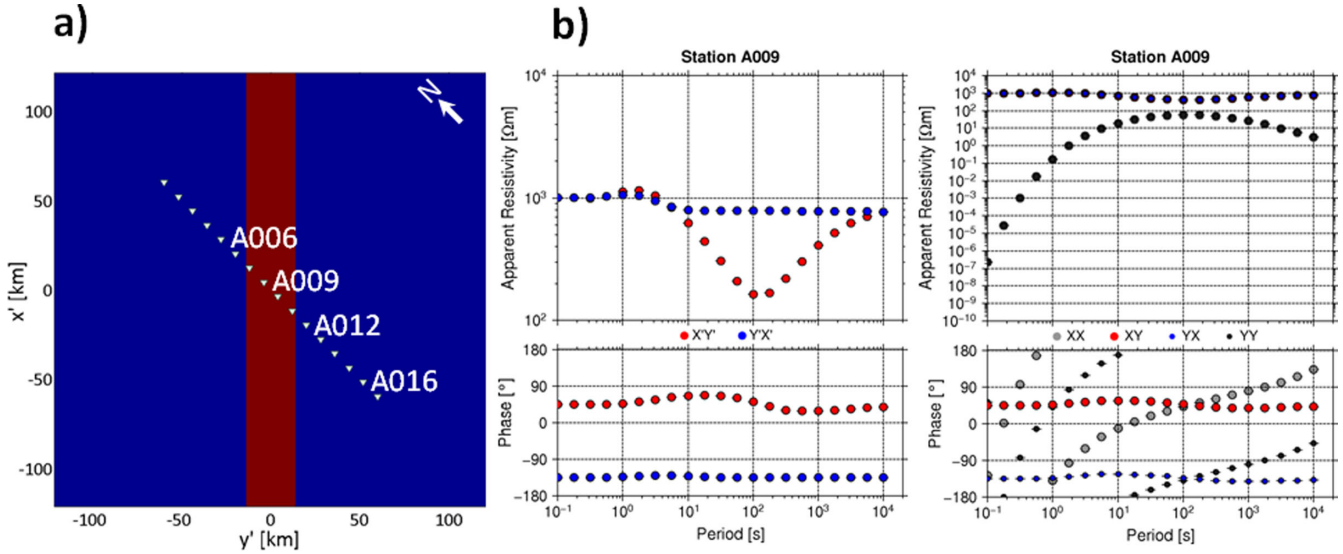

Figure 1. (a) Plan view of the synthetic model used to generate MT data. The white triangles represent the site locations. The model consists of 10 Ωm conductor with a strike direction of 45° east of north in a homogeneous halfspace of 1000 Ωm. (b) Resistivity and phase curves calculated at site A009, the forward response of the test model (x'-axis pointing parallel to strike direction) and in the geographic coordinate system (x-axis points towards north), respectively.

2-D strike. (Note on coordinate systems used: x and y are in the geographic coordinate system, with x directed north and y directed east. x' and y' define the coordinate system of the body, with x' parallel to the body direction, i.e. directed NE for the particular example considered in this paper in a geographic reference frame, and y' directed perpendicular to the body, i.e. NW.)

2 SYNTHETIC DATA: TEST MODEL

To simulate a 2-D case, we designed a simple model consisting of a 10 Ωm conductive body of infinite extent embedded in a homogeneous, 1000 Ωm half space. Fig. 1(a) shows the design of the structure in plan view. The width of the body is 28 km and its depth extent is from 20 to 40 km below the surface. The model is discretized on a 63 × 63 × 45 mesh (including 10 air layers), with a horizontal centre cell size of 4 × 4 km. The central part comprises a uniform horizontal mesh of 43 × 43. On each of the north, south, east and west directions, the central part of the mesh was surrounded by 10 planes, where each successive padding cell was scaled by a factor of 1.5.

Instead of rotating the body with a strike direction of 45° east of north, which would introduce 'corners' on the step-like edges of the body, we rotated the 3-D inversion mesh by 45° west of north. A profile of 16 sites, shown as white solid triangles in Fig. 1(a), is considered. The MT response of the model at 20 periods (four periods per decade), between 0.1 and 10 000 s, was calculated using the 3-D forward modelling code of Mackie *et al.* (1994) (implemented in Geosystems WinGLink package) to generate the four complex components ($\mathbf{Z}_{x'x'}, \mathbf{Z}_{x'y'}, \mathbf{Z}_{y'x'}, \mathbf{Z}_{y'y'}$) of the impedance tensor. In addition, we also calculated the 2-D forward responses of the test model to verify the 3-D forward solution (see Appendix, Fig. A1). 2.5 per cent Gaussian-distributed random noise and scatter were added to the synthetic impedance data (equivalent to 5 per cent to apparent resistivity and 1.5° to phase) and to the error estimates themselves. Fig. 1(b) shows apparent resistivity and phase curves of site A009: (on the left) data are provided in a coordinate system that is aligned with the geo-electric strike direction (forward response of the test model, Fig. 1a) and (on the right) data are shown in a coordinate system that is aligned with geographic directions, that is the x-axis points towards geographic north.

3 3-D INVERSE MODELLING

We inverted the synthetic data from the single profile employing the parallel version of Modular system for ElectroMagnetic inversion (ModEM; Egbert & Kelbert 2012). We considered two different types of coordinate systems summarized below. For the geographic coordinate system, we performed two types of inversions: for the off-diagonal tensor elements only, and for the complete impedance tensor. For the geo-electric strike oriented coordinate system, we ran inversion with off-diagonal components only, and with the complete tensor, but here we only report on the former (see below).

3.1 Model set-up

In the first inversion set-up, we used a coordinate system with the x- and y-axis pointing towards geographic north and east, respectively. The 3-D solution mesh comprised 66 × 67 × 45 cells in the north–south, east–west and vertical directions, with a horizontal cell size of 4 × 4 km in the area of interest. The lateral extent of the padding cells, 11 in each of north, south, east and west directions, successively increased by factor of 1.5. The centre of the mesh, where the horizontal dimensions of the cells were all the same, comprised 45 × 44 × 45 cells. The thickness of the top layer was 50 m, and the thickness of each subsequent layer increased with a vertical factor of 1.2. As input data, which were used in the geographic coordinate system shown in Fig. 2 with pink colour, we ran the inversion twice, once with only the off-diagonal components and a second time with all four complex tensor elements.

In a second inversion set-up, we used the synthetic model configuration (Fig. 1a) that was aligned with the regional geo-electric strike direction, that is x' points 45° east of x. Details of the

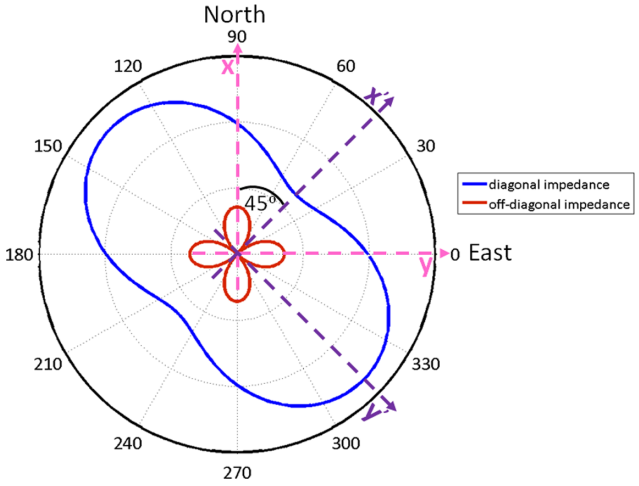

Figure 2. Impedance magnitude rotation diagram (peanut diagram) for site A009 is at 100 s. The blue solid curve represents the off-diagonal impedance element, and the red solid curve represents the diagonal impedance element.

3-D mesh are described in Section 2. In this case, we considered inversion of only the off-diagonal terms, which were also rotated to the strike direction, presented in Fig. 2 with purple colour.

For all the inversions presented in the framework of this paper, the starting model was a homogeneous half-space of 500 Ωm, and the error floors were set as an absolute value to 2.5 per cent of $(|\mathbf{Z}_{xy} \times \mathbf{Z}_{yx}|)^{1/2}$. Note that this error floor setting dominates over the assigned error floors for the diagonal terms and ensures that the diagonal terms are not unduly weighted.

3.2 Smoothing parameter

Smoothing in ModEM is governed by the covariance parameter, which controls the decorrelation length scale, and therefore the resulting roughness of the model. This in effect defines the relative weighting coming from different wavelengths features in the model.

ModEM allows smoothing over different length scales for the *x*-, *y*- and *z*-directions, which is similar to WSINV3DMT (Siripunvaraporn *et al.* 2005a). If no further information is given, this parameter is set to 0.3 in all directions. We carried out tests with several variations on the model covariance to investigate the impact of it on the resulting inversions. Fig. 3 summarizes the final inversion models for various values of model smoothing parameters. In all resulting inversion models, the linear conductive structure is present; however, the extent and intensity of the conductor varies depending on the choice of the smoothing values. Applying lower regularization in the vertical direction (Figs 3A and B) produces a less pronounced conductive feature at 30-km depth. In addition, with lower regularization in the horizontal directions the linear conductive feature tends to lean towards the NNW-SSE direction, whereas with higher smoothing (Figs 3E and F) it leans towards the NNE-SSW direction. The slight skewness of the conductor, that is the slightly the NNW to SSE orientation of the conductor, is because of the location of the stations (as the stations in the NW region, relative to the centre point are closer in proximity to the northern part of the conductor than the southern, as a result, the inversion is assigning the conductivity slightly closer to the station than it ideally should.)

For all inversions discussed in the following section, the same model smoothing (model covariance parameters) value of 0.4 was applied in the *x*- and *y*-directions and a value of 0.1 was applied in the *z*-direction.

3.3 3-D inversion results

The final models obtained by inverting (i) only the off-diagonal elements and (ii) the full impedance tensor elements, are shown in Fig. 4. Whereas the 45° oblique structure has been recovered successfully when inverting the full impedance tensor, for the off-diagonal impedance tensor inversion results the structure is barely sensed, and has not been resolved. As we invert data from a single profile, the along-strike extent of the oblique conductivity structure imaged beneath the profile is resolved to some extent when using all elements. Figs 5(A) and (B) show a comparison of apparent resistivity and phase pseudo-sections for the observed data and the corresponding calculated data for the final inversion results using off-diagonal components and the complete impedance tensor, respectively. The total rms misfits of 1.26 and 1.00 were achieved for each case.

In order to recover the true model using only off-diagonal elements of the impedance tensor, the coordinate system must be considered, meaning that the data set and the model grid should be rotated to a specific coordinate system that is most consistent with a previously identified geo-electrical strike direction (Fig. 6). Off-diagonal apparent resistivity and phase pseudo-sections for the inversion result shown in Fig. 6 and for the observed data were summarized in Fig. 7. An rms misfit of 1.03 was obtained for the model.

Fig. 2 illustrates the polar diagram at 100 s of one of the stations located on top of the conductor. As expected for perfect 2-D geometry, the amplitude of the diagonal term displays a four-leaf clover pattern with zeros in the direction of strike and perpendicular to strike, whereas the off-diagonal term reaches maxima and minima in those directions. In our example, when we invert data in the coordinate frame 45° to strike, the off-diagonal terms reach their maximum and minimum values (Fig. 2, purple solid circles), in which inversion with rotated data was able to recover the true structure well (Fig. 6). In contrast, in the original coordinate system, shown by the pink circles, $|\mathbf{Z}_{xy}|$ is almost the same as $|\mathbf{Z}_{yx}|$, so the response of the conductive anomaly has disappeared (Fig. 4).

Without data and mesh rotation, but with two additional profiles, the inversion results using off-diagonal terms can recover the right geometry of the oblique structure, although the resistivity value shows some discrepancies compared to the true model (Fig. 8). As shown in Fig. 2 (pink solid circles), this result can be explained by not using minimum and maximum values of the off-diagonal terms. Additionally, the model resulting from the inversion using full impedance tensor information from three profiles represent the true model successfully (Fig. 9). Figs 10–13 illustrate the fits of predicted data for the inversion results shown in Figs 8 and 9 to the observed data. The total rms misfits of 1.06 (only off-diagonal elements) and 1.02 (all impedance tensor elements) were obtained.

We also inverted all four elements of the data in the rotated coordinate frame. Not surprisingly, given that the diagonal terms are zero (plus error), we obtained exactly the same result as for inverting the off-diagonals only in the rotated reference frame.

4 CONCLUSIONS

We have applied 3-D MT inversion scheme using non-linear conjugate gradients inversion code of Egbert & Kelbert (2012) to MT

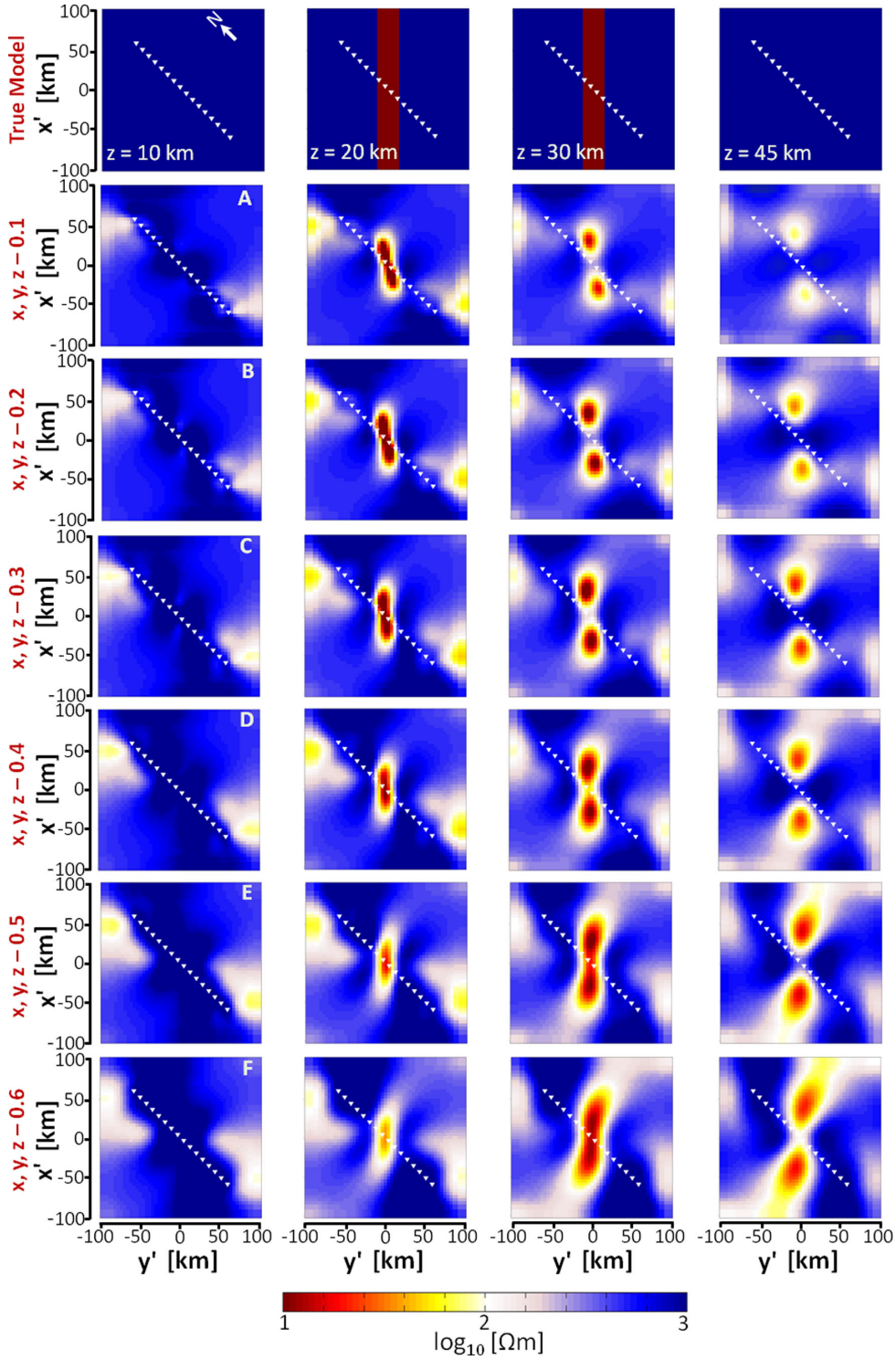

Figure 3. 3-D inversion results of the test model using different smoothing paramaters. As input data, only off-diagonal impedance components ($\mathbf{Z}_{x'y'}$, $\mathbf{Z}_{y'x'}$) were used. The white triangles represent the site locations.

profile data, considering the case of a dominant 2-D oblique conductor buried in a resistive host. Our numerical experiments with 3-D inversion suggest that, if only off-diagonal components are used, such as by Sasaki & Meju (2006), Tuncer *et al.* (2006), Newman *et al.* (2008), and Zhdanov *et al.* (2010), one has to rotate both the 3-D grid and the data to predominant strike to obtain the true resistivity and true geometry of the structure. On the other hand, if the complete impedance tensor is used in the inversion without rotation of coordinate system and data, such as by Farquharson & Craven (2009), the true structure can be clearly mapped, as in this case, the along-strike variation is defined by main diagonal terms.

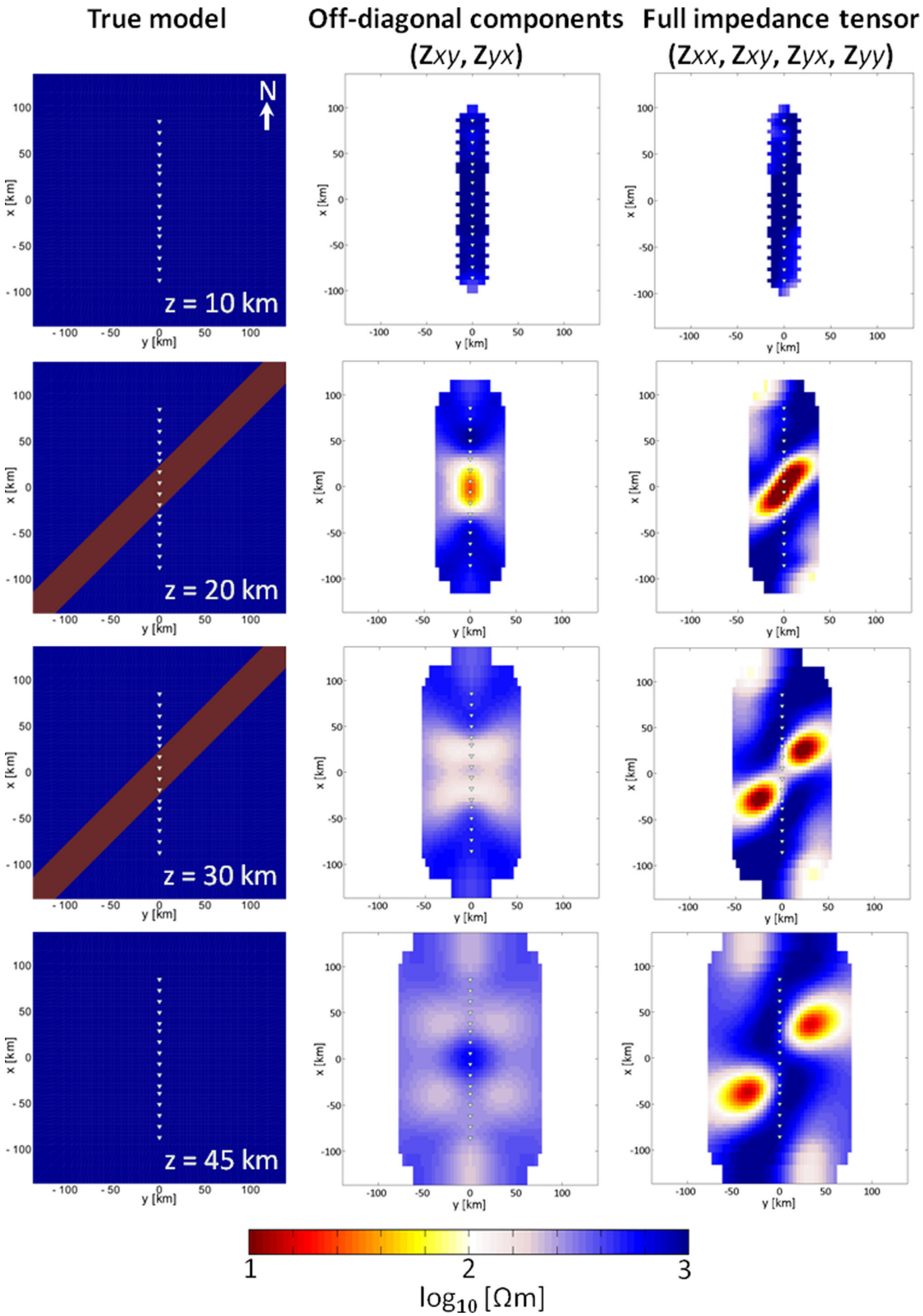

Figure 4. 3-D inversion results of the test model obtained in geographic coordinate system. From left to right the true model and models obtained from inversion of off-diagonal tensor components and from inversion of full impedance tensor. The white triangles represent the site locations.

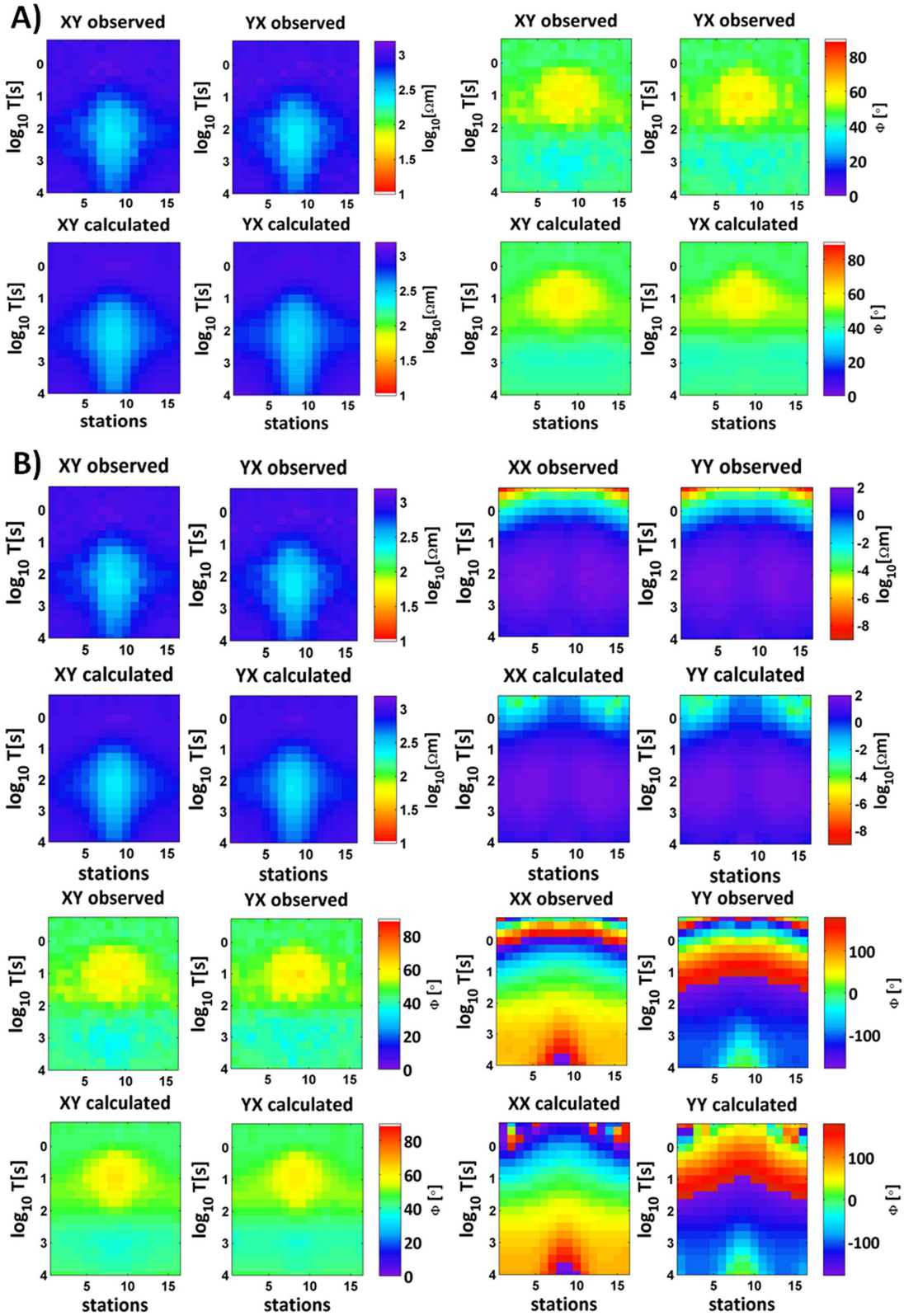

Figure 5. (A) Apparent resistivity and phase pseudo-sections of observed data, and the corresponding predicted data for the final 3-D inversion result fitting off-diagonal data only. (B) Observed and predicted pseudo-sections from the full-tensor 3-D inversion. The total rms misfits of 1.26 and 1.00 were achieved, respectively.

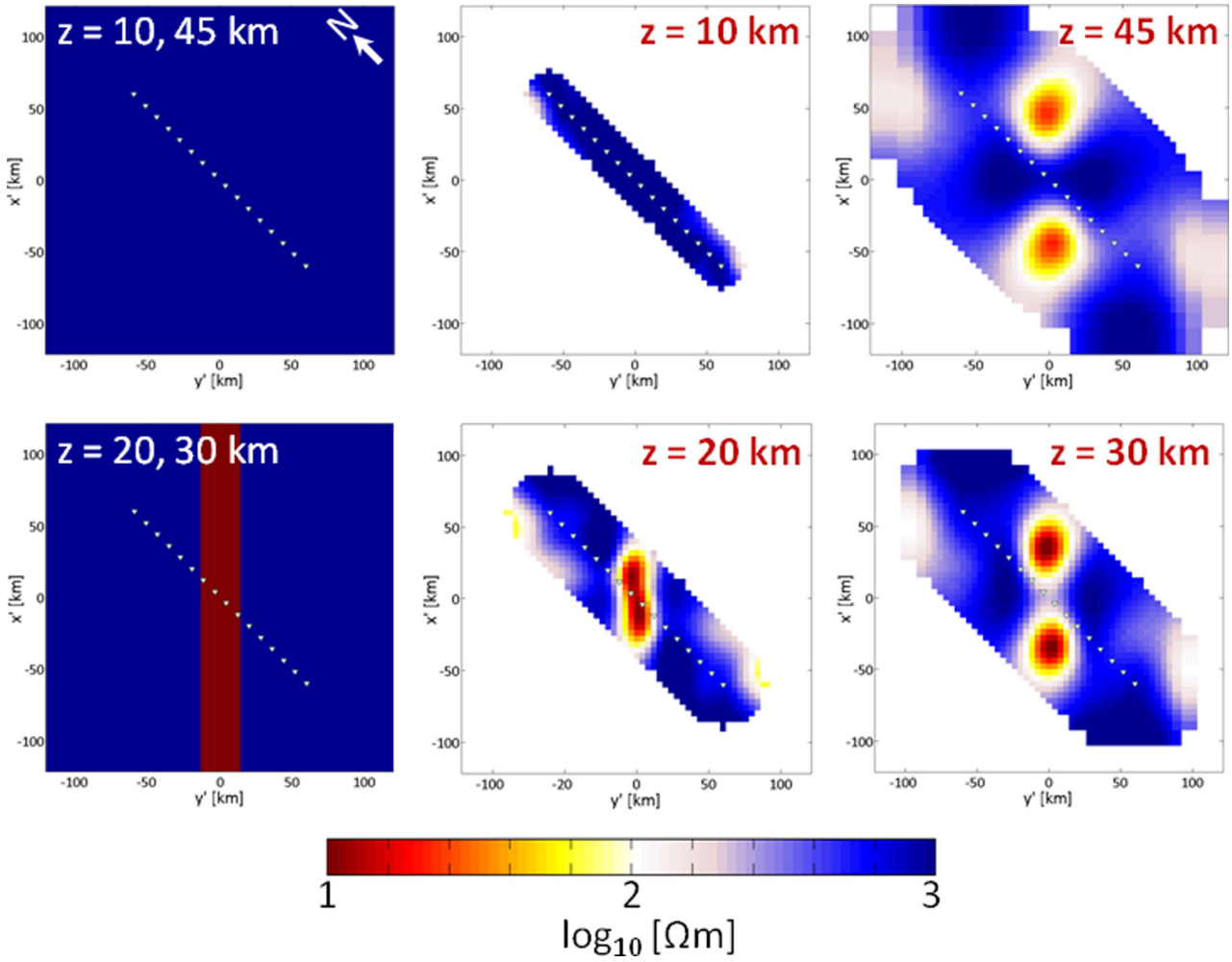

Figure 6. Inversion results obtained using off-diagonal ($\mathbf{Z}_{x'y'}$, $\mathbf{Z}_{y'x'}$) tensor components after aligning both the 3-D mesh and the data with predominant strike direction.

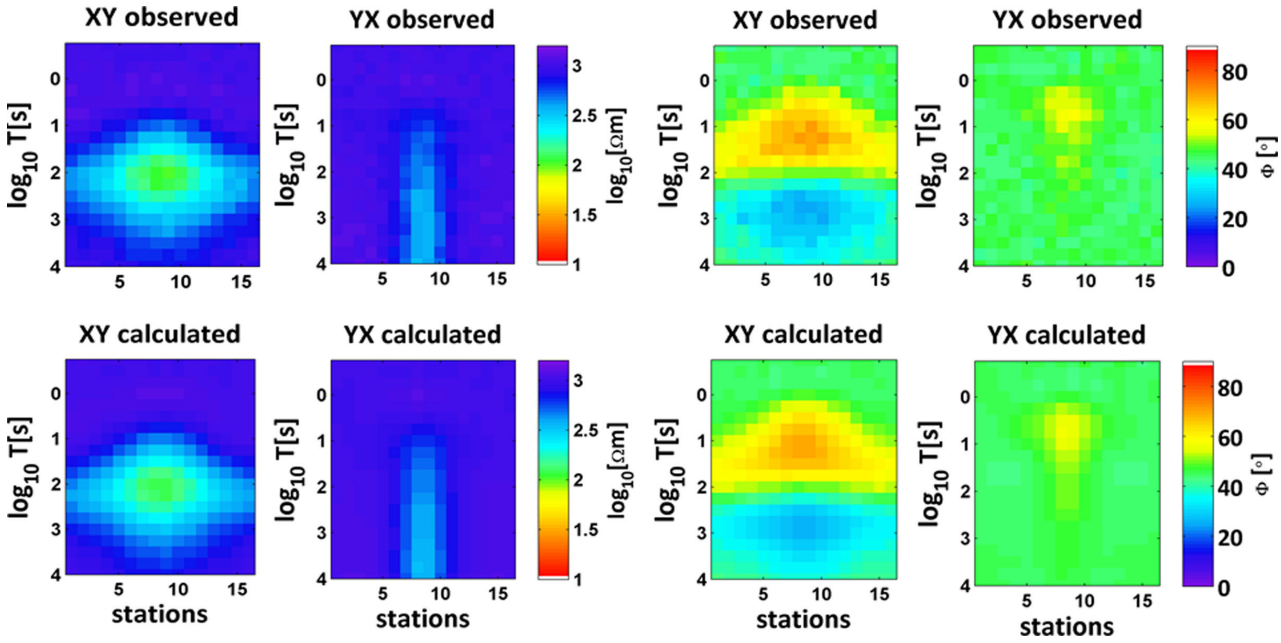

Figure 7. Apparent resistivity and phase pseudo-sections for observed data, and the predicted data for the final 3-D inversion result obtained by fitting off-diagonal components. The total rms misfit of 1.03 was achieved.

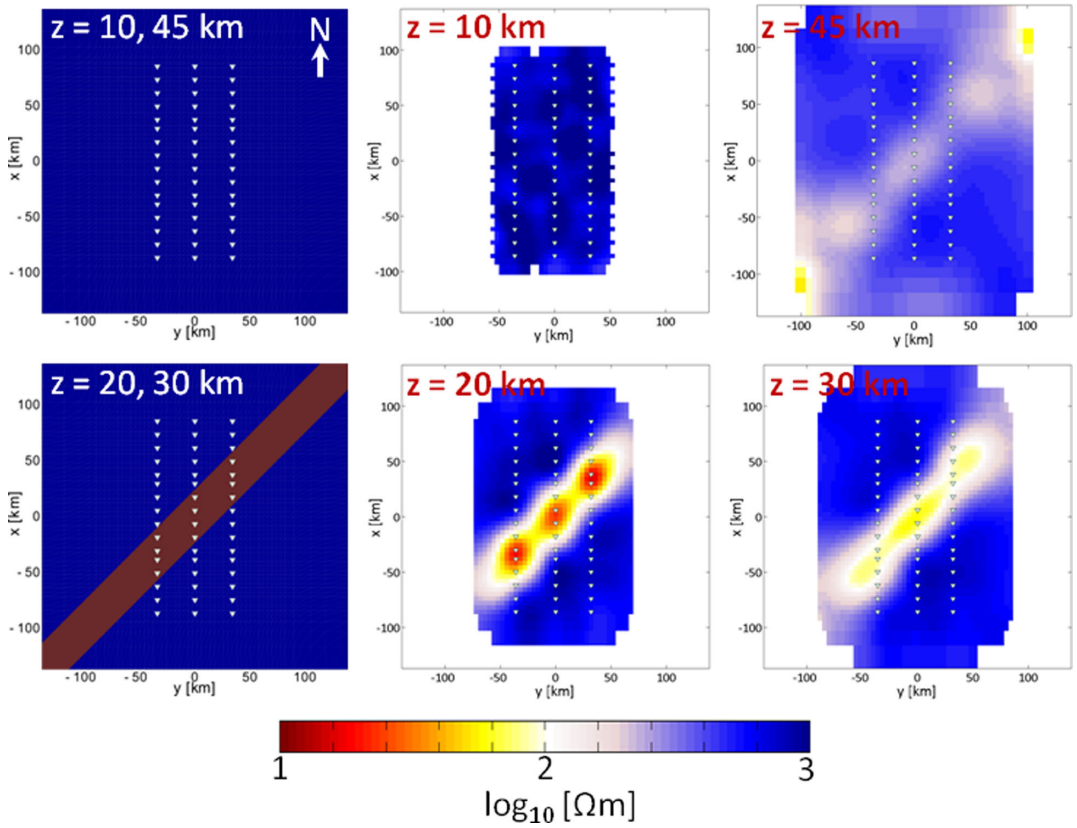

Figure 8. Inversion results from three parallel profiles using only off-diagonal elements ($\mathbf{Z}_{xy}$, $\mathbf{Z}_{yx}$) of the impedance tensor. The white triangles represent the site locations.

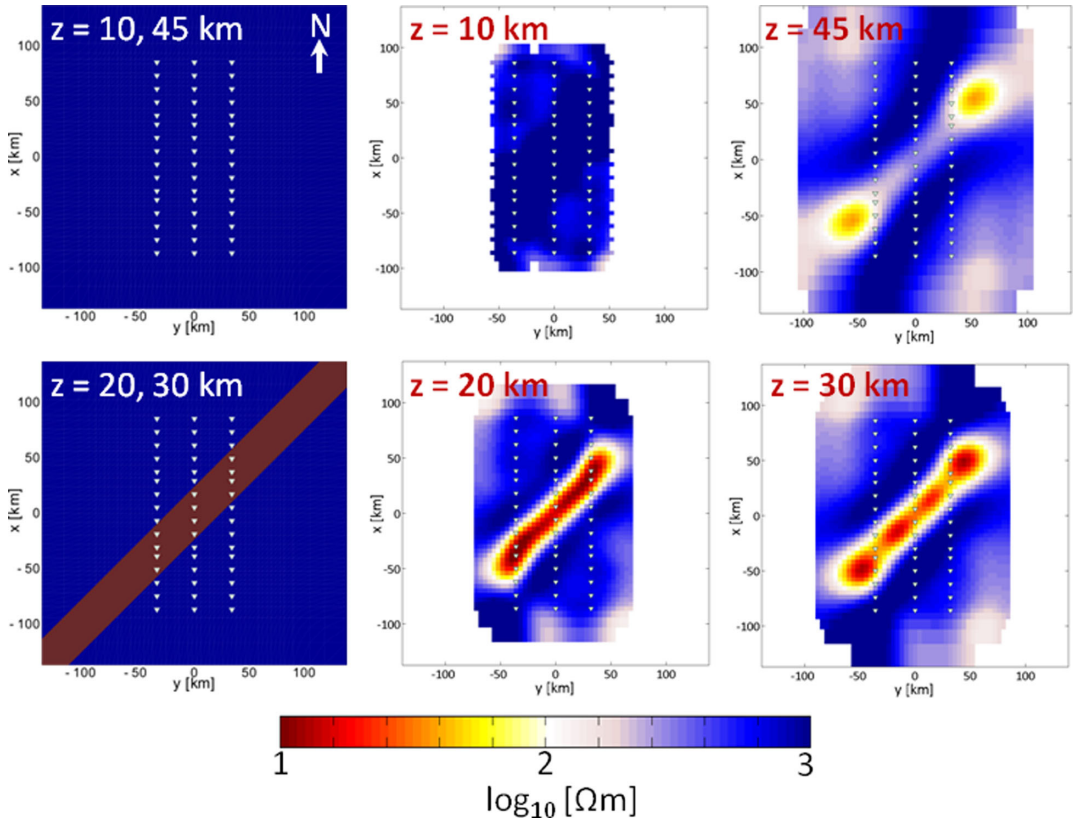

Figure 9. Inversion results from three parallel profiles using complete impedance tensor elements ($\mathbf{Z}_{xx}$, $\mathbf{Z}_{xy}$, $\mathbf{Z}_{yx}$, $\mathbf{Z}_{yy}$). The white triangles represent the site locations.

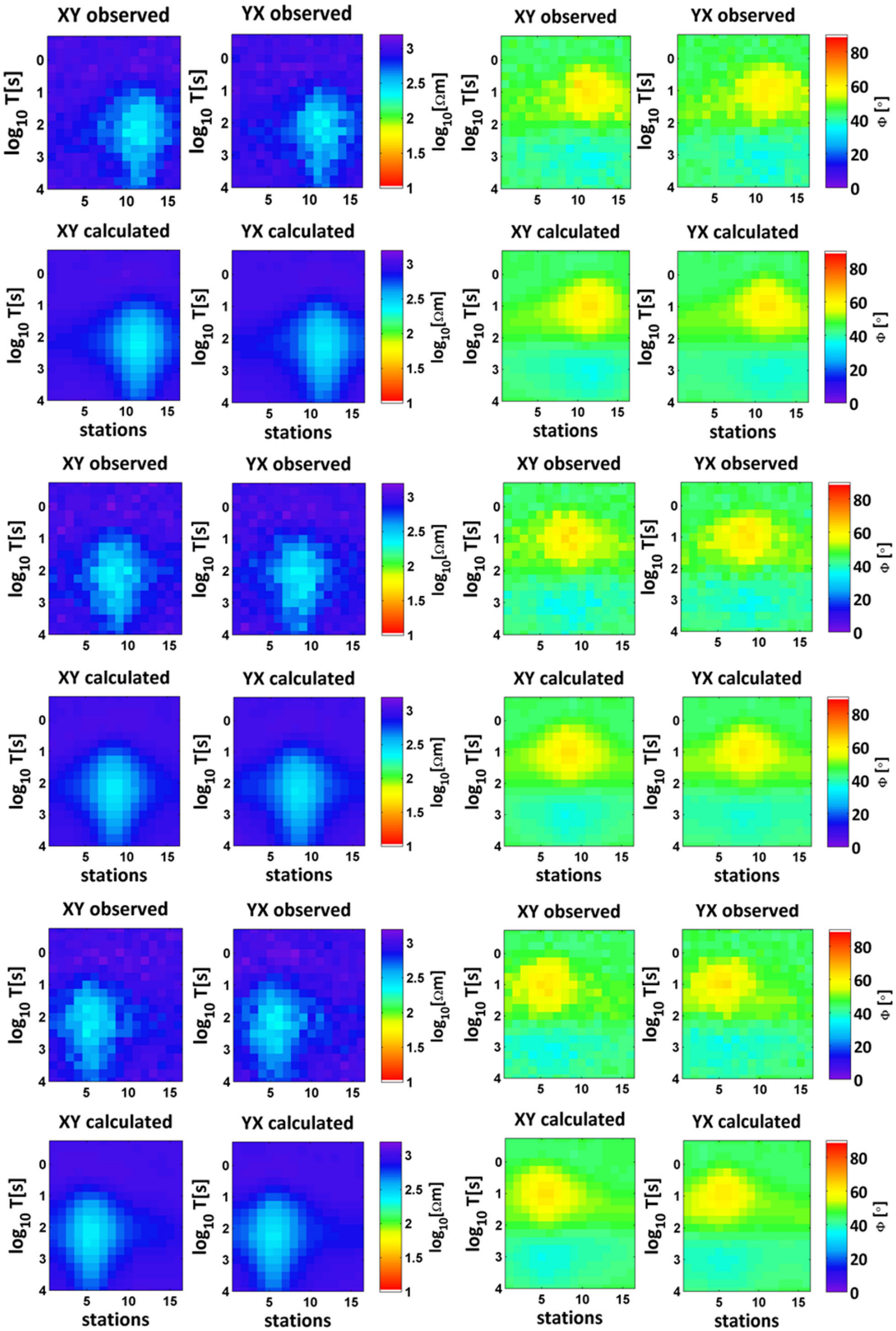

Figure 10. From top to bottom, observed and the predicted pseudo-sections of apparent resistivity and phase for the inversion of the off-diagonal components for left hand-side, centre and right hand-side profiles, respectively. The total rms misfit of 1.06 was achieved.

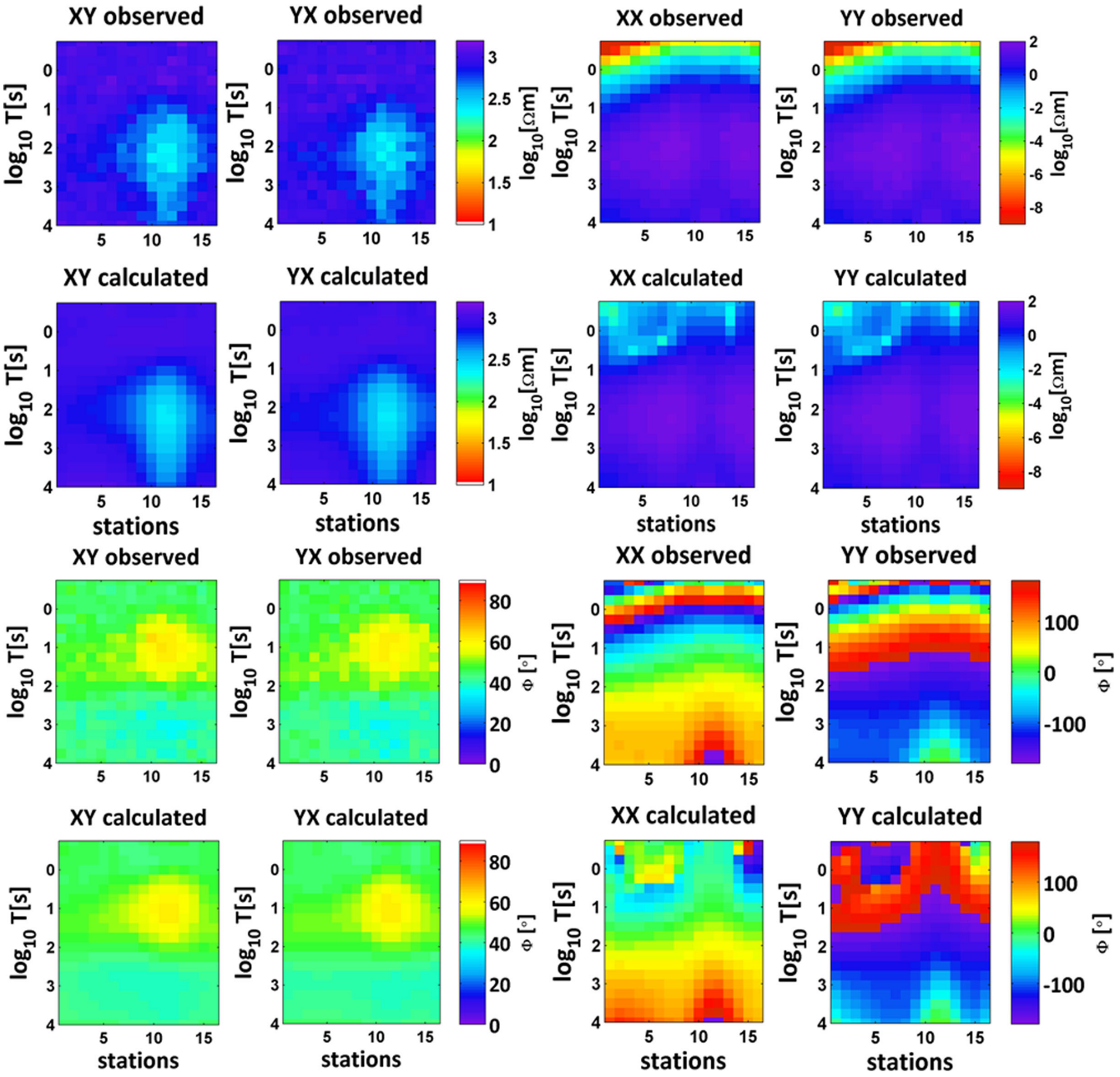

Figure 11. Apparent resistivity and phase pseudo-sections of observed data, and the predicted data for the final 3-D inversion result fitting full-tensor components for the left hand-side profile. The total rms misfit of 1.02 was achieved.

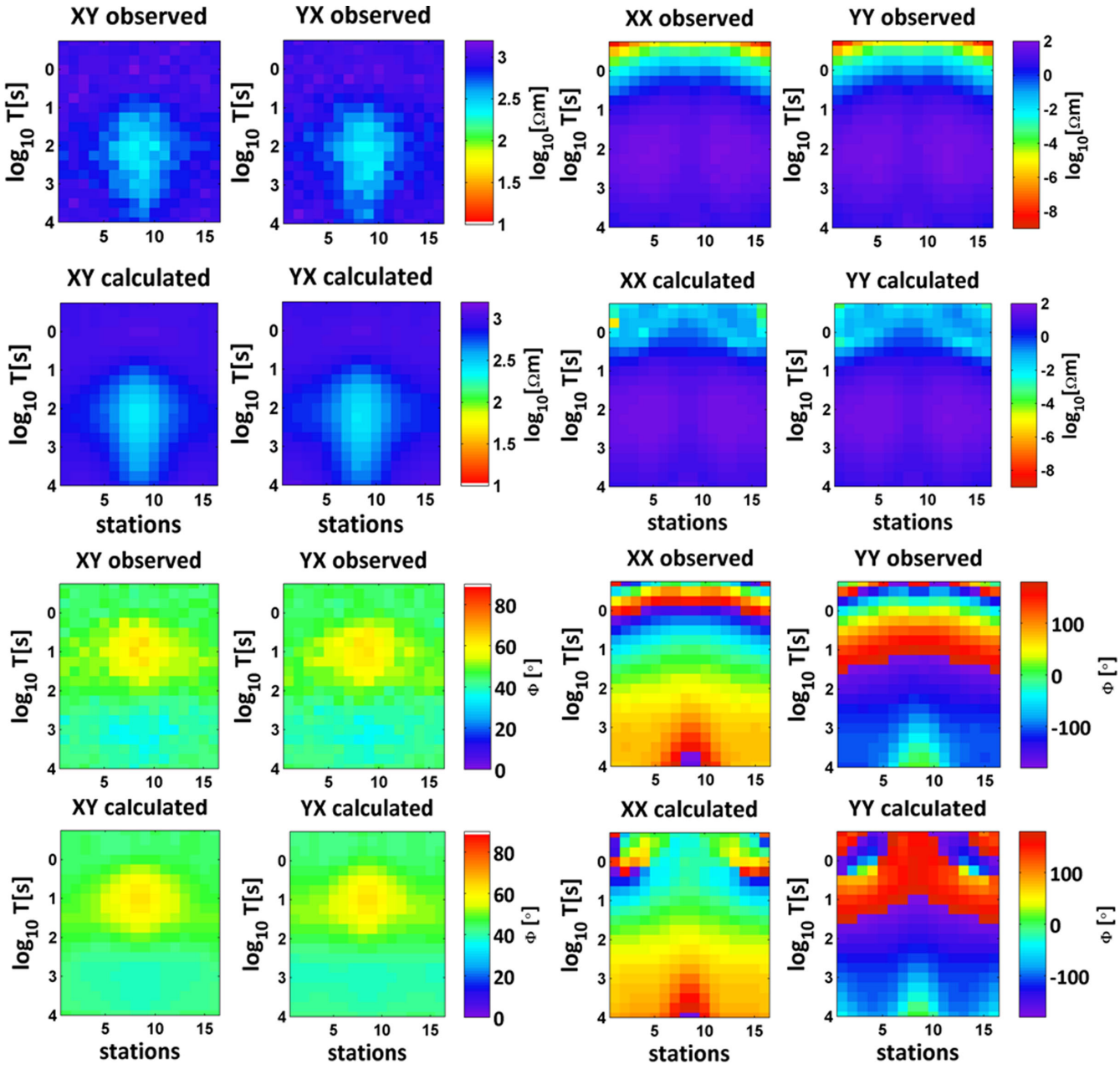

Figure 12. As in Fig. 11, but for the centre profile.

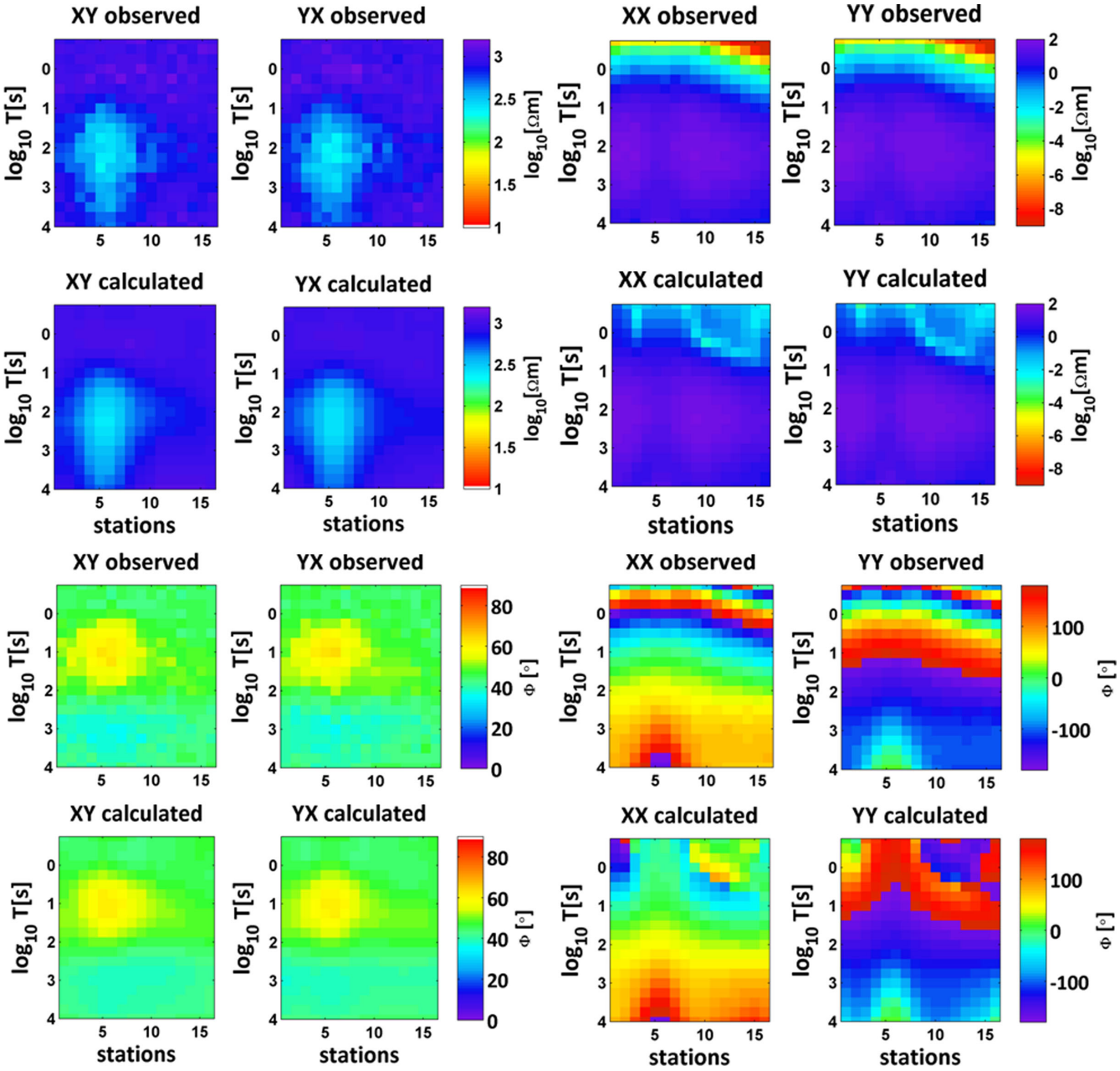

Figure 13. As in Figs 11 and 12, but for the right hand-side profile.

ACKNOWLEDGEMENTS

We wish to acknowledge the financial support of Irish Research Council for Science, Engineering & Technology and Science Foundation Ireland (08/RFP/GEO1693). This work was carried out under the auspices of the TopoMed project in the TOPO-EUROPE EUROCORES and under the PICASSO project. We thank Gary Egbert (the editor), Colin Farquharson and Yoonho Song for their helpful comments on the original version of this manuscript that improved it. Finally, we thank the Irish Centre for High Performance Computing (ICHEC) for availing the STOKES cluster to carry out the numerical computations. Gary Egbert is thanked for providing the ModEM code. Naser Meqbel is thanked for aiding Jan Vozar in installing the code on our clusters.

REFERENCES

Bertrand, E.A. *et al.*, 2012. Magnetotelluric imaging beneath the Taiwan orogen: an arc-continent collision, *J. geophys. Res.,* **117**(B1), B01402, doi:10.1029/2011JB008688.

Egbert, G.D. & Kelbert, A., 2012. Computational recipes for electromagnetic inverse problems, *Geophys. J. Int.,* **189,** 251–267.

Farquharson, C., Oldenburg, D., Haber, E. & Shekhtman, R., 2002. An algorithm for the three-dimensional inversion of magnetotelluric data, *SEG Technical Program Expanded Abstracts,* Society of Exploration Geophysicists.

Farquharson, C.G. & Craven, J.A., 2009. Three-dimensional inversion of magnetotelluric data for mineral exploration: an example from the McArthur River uranium deposit, Saskatchewan, *J. appl. Geophys.,* **68,** 450–458.

Khoza, D., Jones, A.G., Muller, M., Evans, R., Webb, S. & Miensopust, M., 2013. Tectonic model of the Limpopo belt: constraints from magnetotelluric data, *Precambrian Res.,* **226,** 143–156.

Kiyan, D., Jones, A.G., Fullea, J., Hogg, C., Ledo, J. & Siniscalchi, A., 2010. Crustal and lithospheric imaging of the Atlas Mountains of Morocco inferred from magnetotelluric data, *AGU Fall Meeting,* abstract T23C-2281.

Mackie, R.L., Smith, J.T. & Madden, T.R., 1994. Three-dimensional electromagnetic modeling using finite difference equations: the magnetotelluric example, *Radio Sci.,* **29,** 923–935.

Marquis, G., Jones, A.G. & Hyndman, R.D., 1995. Coincident conductive and reflective middle and lower crust in southern British Columbia, *Geophys. J. Int.,* **120,** 111–131.

Miensopust, M.P., Jones, A.G., Muller, M.R., Garcia, X. & Evans, R.L., 2011. Lithospheric structures and Precambrian terrane boundaries in northeastern Botswana revealed through magnetotelluric profiling as part of the Southern African magnetotelluric experiment, *J. geophys. Res.,* **116**(B2), 1–21.

Newman, G.A., Gasperikova, E., Hoversten, G.M. & Wannamaker, P.E., 2008. Three-dimensional magnetotelluric characterization of the Coso geothermal field, *Geothermics,* **37,** 369–399.

Patro, P.K. & Egbert, G.D., 2011. Application of 3D inversion to magnetotelluric profile data from the Deccan Volcanic Province of Western India, *Phys. Earth planet. Inter.,* **187,** 33–46.

Rodi, W. & Mackie, R.L., 2001. Nonlinear conjugate gradients algorithm for 2-D magnetotelluric inversion, *Geophysics,* **66,** 174–187.

Sasaki, Y. & Meju, M.A., 2006. Three-dimensional joint inversion for magnetotelluric resistivity and static shift distributions in complex media, *J. geophys. Res.,* **111**(B5), B05101, doi:10.1029/2005JB004009.

Siripunvaraporn, W., Egbert, G., Lenbury, Y. & Uyeshima, M., 2005a. Three-dimensional magnetotelluric inversion: data-space method, *Phys. Earth planet. Inter.,* **150,** 3–14.

Siripunvaraporn, W., Egbert, G. & Uyeshima, M., 2005b. Interpretation of two-dimensional magnetotelluric profile data with three-dimensional inversion: synthetic examples, *Geophys. J. Int.,* **160,** 804–814.

Tietze, K. & Ritter, O., 2013. Three-dimensional magnetotelluric inversion in practice–the electrical conductivity structure of the San Andreas Fault in Central California, *Geophys. J. Int.,* **195,** 130–147.

Tuncer, V., Unsworth, M.J., Siripunvaraporn, W. & Craven, J.A., 2006. Case history exploration for unconformity-type uranium deposits with audiomagnetotelluric data: a case study from the McArthur River mine, Saskatchewan, Canada, *Geophysics,* **71**(6), B201–B209.

Xiao, Q., Cai, X., Xu, X., Liang, G. & Zhang, B., 2010. Application of the 3D magnetotelluric inversion code in a geologically complex area, *Geophys. Prospect.,* **58,** 1177–1192.

Zhdanov, M.S., Green, A., Gribenko, A. & Cuma, M., 2010. Large-scale three-dimensional inversion of EarthScope MT data using the integral equation method, *Phys. Solid Earth,* **46,** 670–678.

APPENDIX: COMPARISON OF 2-D AND 3-D FORWARD RESPONSES

To compare the responses of 3-D forward modelling with 2-D solutions, we simulate the same structure using a 2-D forward algorithm, the code of Rodi & Mackie (2001) (implemented in Geosystems WinGLink package). Calculated 2-D responses were rotated by 45° to gain the diagonal components ($|\mathbf{Z}_{xx}|$, $|\mathbf{Z}_{yy}|$) of the impedance tensor. All four components of the rotated 2-D (blue circle) and 3-D (red star) are shown in Fig. A1.

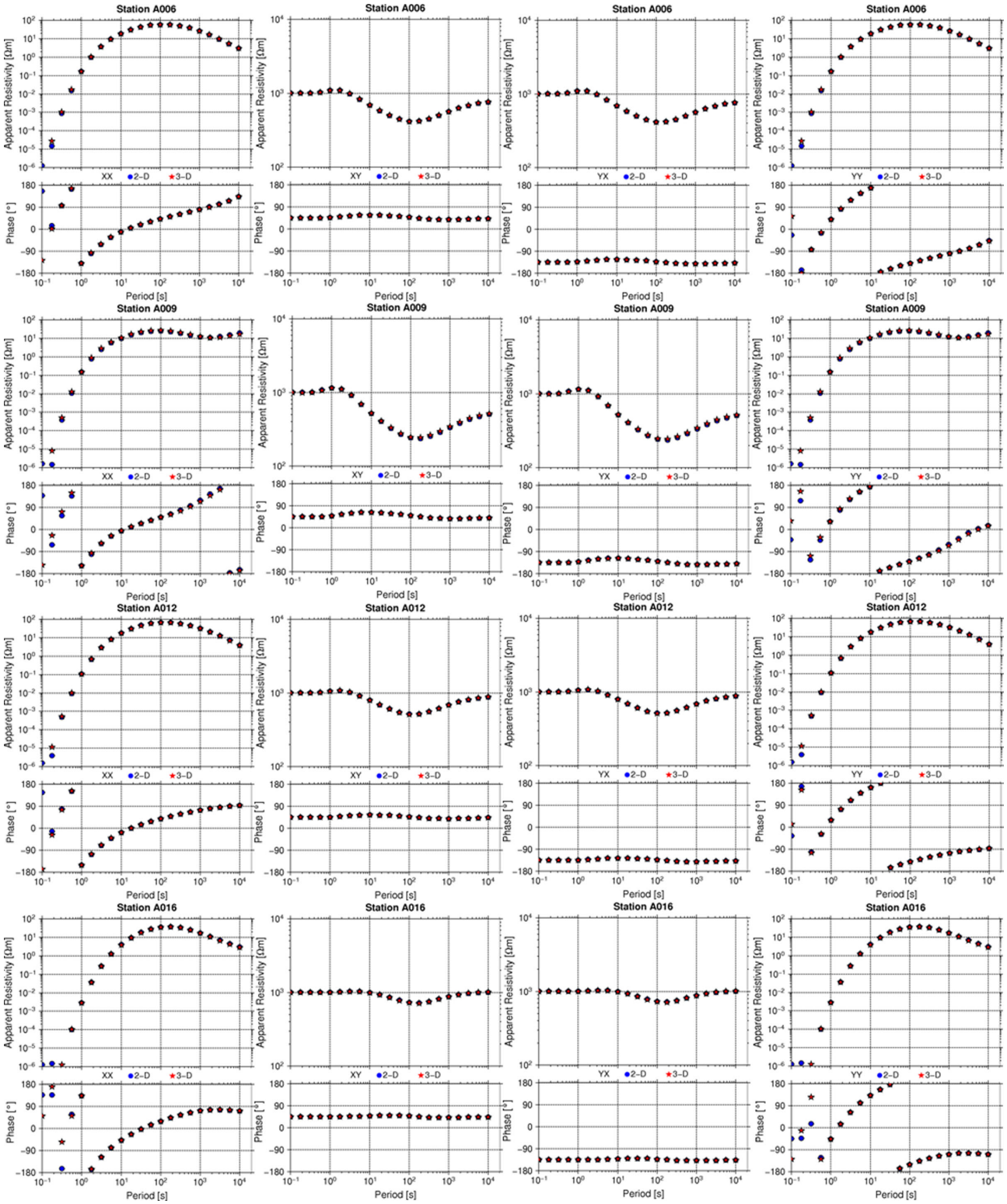

Figure A1. Comparison of the rotated 2-D and 3-D responses. Resistivity and phase curves for all four components calculated at stations A006, A009, A012 and A016. The blue circles represent the rotated 2-D responses into strike angle of 45° and the red stars are the 3-D responses.